




Magnetic field induced antiferromagnetic cone structure in multiferroic BiFeO₃M. Matsuda , S. E. Dissanayake*, and T. Hong*Neutron Scattering Division, Oak Ridge National Laboratory, Oak Ridge, Tennessee 37831, USA*Y. Ozaki and T. Ito *National Institute of Advanced Industrial Science and Technology (AIST), Tsukuba, Ibaraki 305-8565, Japan*M. Tokunaga *The Institute for Solid State Physics (ISSP), The University of Tokyo, Kashiwa, Chiba 277-8581, Japan*

X. Z. Liu

*Helmholtz-Zentrum Berlin für Materialien und Energie, Hahn-Meitner Platz 1, D-14109 Berlin, Germany
and School of Physics, Sun Yat-Sen University, Guangzhou 510275, People's Republic of China*M. Bartkowiak  and O. Prokhnenko *Helmholtz-Zentrum Berlin für Materialien und Energie, Hahn-Meitner Platz 1, D-14109 Berlin, Germany*

(Received 27 January 2020; accepted 6 March 2020; published 31 March 2020)

Neutron diffraction measurements were performed under high magnetic fields up to 17 T in a multiferroic BiFeO₃ single crystal, in which an intermediate magnetic (IM) phase has been found between the cycloid and canted antiferromagnetic phases [S. Kawachi *et al.*, *Phys. Rev. Mater.* **1**, 024408 (2017)]. We clearly found that the incommensurate magnetic peaks, which split perpendicular to the magnetic field in the cycloid phase, rotate by 90 deg to align parallel to the field in the IM phase. The magnetic structure in the IM phase can be best described by an antiferromagnetic cone (AF cone) structure. The transition from the cycloid to AF cone is of first order and the direction of the magnetic wave vector and the easy plane of the cycloidal component are rotated by 90 deg without changing the cycloidal modulation period, whereas the transition from the AF cone to canted antiferromagnetic phase is gradual and the cone angle becomes smaller gradually without changing the modulation period. Interestingly, the cycloidal component as well as the cone angle in the IM phase shows a large hysteresis between the field increasing and decreasing processes. This result, combined with the magnetostriction with a large hysteresis previously reported in the IM phase, suggests a strong magnetoelastic coupling.

DOI: [10.1103/PhysRevMaterials.4.034412](https://doi.org/10.1103/PhysRevMaterials.4.034412)**I. INTRODUCTION**

BiFeO₃, a rare multiferroic compound that shows antiferromagnetism and ferroelectricity simultaneously above room temperature, has been studied intensively [1,2] because of its rich physics and potential device application. BiFeO₃ crystallizes in a rhombohedral structure (*R3c*). The structure is also represented by a pseudocubic structure with $a \sim 3.96 \text{ \AA}$ and $\alpha \sim 89.4^\circ$ which will be used in this paper. This material shows a high Curie temperature of $T_c \sim 1100 \text{ K}$, below which ferroelectricity appears [3]. A cycloidal magnetic order develops below $T_N \sim 640 \text{ K}$ [4] [Fig. 1(a)]. There are three equivalent magnetic domains, in which the magnetic propagation vectors are $(\delta, -\delta, 0)$, $(\delta, 0, -\delta)$, and $(0, -\delta, \delta)$ with the easy planes perpendicular to $[1, 1, -2]$, $[1, -2, 1]$, and $[-2, 1, 1]$, respectively. A slight anharmonicity of the cycloid structure was suggested [5,6]. Applying magnetic field, various experimental results indicate a magnetic transition around

20 T [7–15] which corresponds to a transition from the incommensurate cycloid structure to a canted antiferromagnetic (CAFM) structure [Fig. 1(c)].

Recently, an intermediate magnetic (IM) phase has been found between the cycloid and CAFM phases [16]. This IM phase, where a large magnetoelectric effect was observed, is considered to originate from the anisotropic magnetic interactions that are coupled to the ferroelectric property. The magnetic structure in the IM phase was predicted to be an antiferromagnetic cone (AF cone) structure theoretically [16], as shown in Fig. 1(b). This phase originates from the competition between two different Dzyaloshinskii-Moriya (DM) interactions (DM vectors along $[1, 1, -2]$ and $[1, 1, 1]$). The DM interaction along $[1, 1, -2]$ is dominant at low fields and gives rise to the cycloid structure [17–19]. The DM interaction along $[1, 1, 1]$ causes a small spin density wave component along $[1, 1, -2]$ [20]. The latter DM interaction becomes more dominant in the IM phase. Since DM interactions are coupled to structural symmetry, the AF cone structure can be strongly affected by the structural distortion.

Neutron diffraction experiments using a vertical-field magnet were performed previously [16]. A magnetic transition

*Present address: Department of Physics, Duke University, Durham, North Carolina 27708, USA.

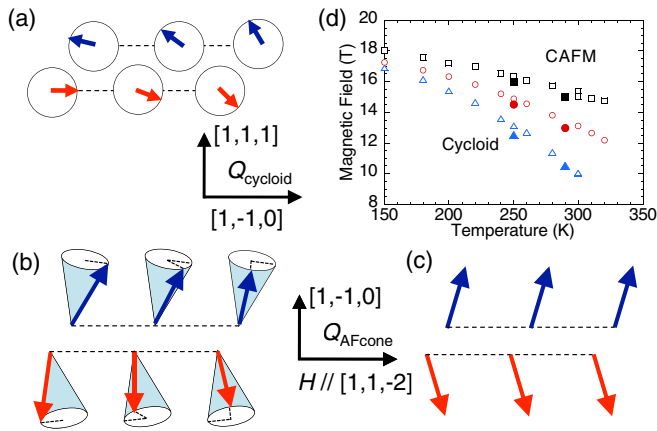


FIG. 1. (a) Cycloid structure at ambient and low magnetic fields, (b) AF cone structure predicted for the intermediate phase theoretically [16], and (c) CAFM structure. The red arrows represent the Fe moments in a triangular plane perpendicular to $[1, 1, 1]$ direction. In the plot the rotation plane includes $[1, 1, 1]$ direction. The blue arrows represent the Fe moments in the adjacent plane along $[1, 1, 1]$. The modulation pitches shown in (a) and (b) and the canting angle in (c) are exaggerated for clarity. (d) Magnetic field-temperature phase diagram. The circles and triangles represent the transition fields between the cycloid and AF cone structure observed in the field increasing and decreasing processes, respectively. The squares represent the transition fields between the AF cone and CAFM structure. Closed and open symbols correspond to the data obtained with neutron diffraction and magnetization measurements, respectively. The magnetization data are from Ref. [16].

to the IM phase was confirmed from a change of the magnetic peak structure from being incommensurate to commensurate. However, due to the experimental configuration with insufficient resolution along the field direction where a commensurate peak is expected to split, it was not possible to unambiguously determine that the magnetic structure in the IM phase is the AF cone structure. It is important to determine the detailed magnetic structure in the IM phase to fully understand the magnetoelectric effect in this material.

We performed neutron diffraction measurements using a single crystal of BiFeO_3 . We first investigated the magnetic domain redistribution, which occurs at low magnetic fields. The three equivalent magnetic domains present at ambient and low magnetic fields was found to merge into a single magnetic domain above 6 T. After that, we measured magnetic field dependence of the peak profile around the $(1/2, 1/2, 1/2)$ magnetic Bragg peak in horizontal magnetic field up to 17 T. We successfully observed incommensurate peaks, which split along the magnetic field direction $[1, 1, -2]$ at the $(1/2, 1/2, 1/2)$ main peak, in the IM phase. The magnetic field and temperature region, where the incommensurate peaks appear, is consistent with that in the phase diagram obtained by the magnetization measurements [16]. We confirmed that the magnetic structure in the IM phase is consistent with the AF cone structure which is predicted theoretically. The cycloidal spin component in the AF cone phase, which shows a large hysteresis between the field increasing and decreasing processes, suggests a strong magnetoelastic coupling.

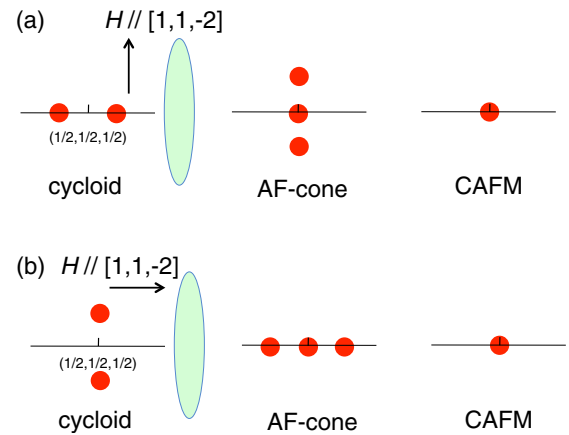


FIG. 2. Configurations of neutron diffraction experiments in vertical magnetic field with $[1, 1, 1]$ - $[1, -1, 0]$ scattering plane (a) and horizontal magnetic field with $[1, 1, 1]$ - $[1, 1, -2]$ scattering plane (b). The filled circles represent magnetic Bragg peaks around $(1/2, 1/2, 1/2)$. The ellipsoid represents the instrumental resolution function schematically. Slightly canted ferromagnetic component in the AF cone and CAFM phases should cause magnetic signal which overlaps to the nuclear Bragg peaks, although the ferromagnetic Bragg peak is not shown here.

II. EXPERIMENTAL DETAILS

A single crystal of BiFeO_3 was grown using the traveling solvent floating zone (TSFZ) method, as described in Ref. [21]. The dimensions of the single crystal is $3\phi \times 10 \text{ mm}^3$. The effective mosaic of the single crystal is about 0.4° with the spectrometer configurations as described below. This is the same crystal used for the high magnetic field neutron diffraction study in Ref. [16]. It should be emphasized that high quality single crystal, which has a good mosaicity of less than 0.4 deg full-width-at-half-maximum, is the key to resolve the incommensurate magnetic peaks both in the cycloid and IM phases. The neutron diffraction measurements in horizontal magnetic fields up to 17 T were performed on HFM/EXED facility at BER II research reactor in Helmholtz-Zentrum Berlin [22]. The single crystal was oriented in the $(1, 1, 1)$ - $(1, 1, -2)$ scattering plane and was mounted in a closed-cycle ^4He gas refrigerator. High static magnetic fields were applied using a hybrid magnet system. The magnetic field was applied up to 17 T horizontally along $[1, 1, -2]$ direction [Fig. 2(b)]. To access the reflections of interest the magnet was rotated by 9 deg with respect to the incident beam. EXED instrument, operated in a time-of-flight diffractometer mode [23], was set to a wavelength range $0.73\text{--}1.88 \text{ \AA}$.

The neutron diffraction experiments in vertical magnetic fields up to 9 T were carried out on a cold triple-axis neutron spectrometer CTAX, installed at the High Flux Isotope Reactor (HFIR) at Oak Ridge National Laboratory (ORNL). Neutrons with a final energy of 5 meV was used, together with a horizontal collimator sequence of guide $20'\text{--}S\text{--}80'\text{--}120'$. Contamination from higher-order beams was effectively eliminated using a cooled Be filter. The single crystal was oriented in the $(1, 1, 1)$ - $(1, -1, 0)$ scattering plane. The magnetic field vertical to the scattering plane was applied along $[1, 1, -2]$ direction [Fig. 2(a)].

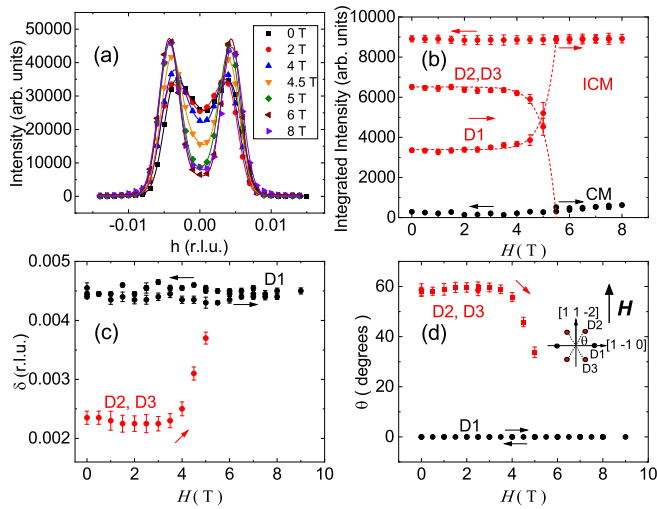


FIG. 3. Orientation of the magnetic domains with $H \parallel [1, 1, -2]$ observed using neutron diffraction. (a) The peak profile along $(1/2 \pm h, 1/2 \mp h, 1/2)$ as a function of magnetic field measured in the field increasing process. (b) Integrated intensities of commensurate and incommensurate magnetic peaks as a function of magnetic field. D1, D2, and D3 represent three magnetic domains shown in the inset of (d). (c) Magnetic field dependence of incommensurability (δ) of the incommensurate magnetic Bragg peaks at $(1/2 \pm \delta, 1/2 \mp \delta, 1/2)$, $(1/2 \mp \delta, 1/2, 1/2 \pm \delta)$, and $(1/2, 1/2 \pm \delta, 1/2 \mp \delta)$. (d) Angle between the cycloidal plane and the scattering plane (θ) as a function of magnetic field. The inset shows the six magnetic incommensurate peaks (filled circles) and θ .

III. EXPERIMENTAL RESULTS AND DISCUSSION

A. Magnetic domains

Neutron diffraction study was performed in a vertical magnetic field in order to investigate the magnetic domain orientation in the field. The experimental configuration shown in the inset of Fig. 3(d) was employed, which is the same as in Refs. [24,25]. Figure 3 shows the result with $H \parallel [1, 1, -2]$ measured at 2 K. At ambient field, there are two peaks around $(1/2 \pm \delta, 1/2 \mp \delta, 1/2)$ with $\delta \sim 0.004$. With increasing magnetic field, the intensity at $(0.5, 0.5, 0.5)$ is reduced between 4 and 5 T, while the incommensurate peaks become more intense and sharper with larger peak separation. The three magnetic domain (D1, D2, and D3) arrangement expected at ambient magnetic field is displayed in the inset of Fig. 3(d). Because of the insufficient Q resolution perpendicular to the scattering plane and very small incommensurability, the out-of-plane peaks are observed as if those are in the scattering plane. The data were fitted with five Gaussian peaks, outer two peaks from D1, inner two peaks from D2 and D3, and a peak at the center. For the analysis we assumed that the cycloidal plane of D1 is in the scattering plane and D2 and D3 have the same δ .

The field dependence of the intensity is plotted in Fig. 3(b). Above 4.5 T, the intensity from D2 and D3 abruptly disappears and that from D1 increases. This is the reason why the peaks become sharper and more intense. With decreasing the field, the intensities at these positions stay almost the same. After the first cycle of field increase and decrease, the field

dependence of the intensities are the same as those in the first field decreasing process. The commensurate peak gradually increase with increasing magnetic field above ~ 5 T. This will be discussed in Sec. III B. Figure 3(c) shows the field dependence of δ of the magnetic Bragg peaks. δ of D2 and D3 stays almost the same up to 4 T and abruptly increases above 4 T. δ can be converted to the angle between the cycloidal plane and the scattering plane (θ) with the relation $\cos^{-1}(\delta/\delta_0)$, where δ_0 is the incommensurability of D1 lying in the scattering plane. At low fields, the cycloidal planes of D2 and D3 are tilted by 60 deg from the scattering plane. θ changes from 60° to 0° at 5.5 T, indicating that D2 and D3 merge to D1. These results are consistent with those in Ref. [26].

After the magnetic domains D2 and D3 merge to D1, the single domain structure is robust unless it is heated above the Néel temperature (640 K). The high magnetic field study, which is described in Sec. III B, was performed using a single crystal with a single magnetic domain (D1).

B. Magnetic field induced transitions

Neutron diffraction study in horizontal magnetic field was performed to clarify the magnetic structure in the IM phase. The experimental configuration shown in Fig. 2(b) was employed. Figure 4 shows the contour map of the magnetic intensity at $(1/2, 1/2, 1/2)$ along $[1, 1, -2]$ direction at 250 and 290 K as a function of magnetic field. As described in Sec. III A, two incommensurate peaks from the cycloid phase, which split along $[1, -1, 0]$, should be present at low fields. However, due to the vertically elongated resolution as shown in Fig. 2(b), the two incommensurate peaks below 5 T, which split along $[1, -1, 0]$, are integrated into a single commensurate peak.

In the field increasing process, shown in Figs. 4(a) and 4(c), additional signals appear at both sides of the commensurate peak around 15 T at 250 K and around 14 T at 290 K. On the other hand, in the field decreasing process, shown in Figs. 4(b) and 4(d), the side peaks appear around 14 T at 250 K and around 13 T at 290 K. The profiles of the central and two side peaks were fitted with three Gaussian functions. The integrated intensities of the commensurate and incommensurate peaks at 250 and 290 K as a function of magnetic field are shown in Figs. 5(a) and 5(b), respectively. The increase of the commensurate magnetic intensity with increasing magnetic field and the hysteresis of the incommensurate magnetic intensity are clearly seen. Figures 5(e) and 5(f) show half of the peak separation of the two incommensurate peaks, which corresponds to the incommensurability δ' of the magnetic peaks at $(1/2 \pm \delta', 1/2 \pm \delta', 1/2 \mp 2\delta')$. We found that the peak separation of the two incommensurate peaks is almost field and temperature independent and has similar values in the field increasing and decreasing processes. Since the incommensurability of the magnetic peaks corresponds to the reciprocal cycloidal periodicity, this results suggest that the cycloidal modulation period keeps about a constant value in the IM phase.

As reported in Ref. [16], the incommensurate magnetic peaks, split perpendicularly to the magnetic field in the cycloid phase, becomes commensurate, indicating that the peak

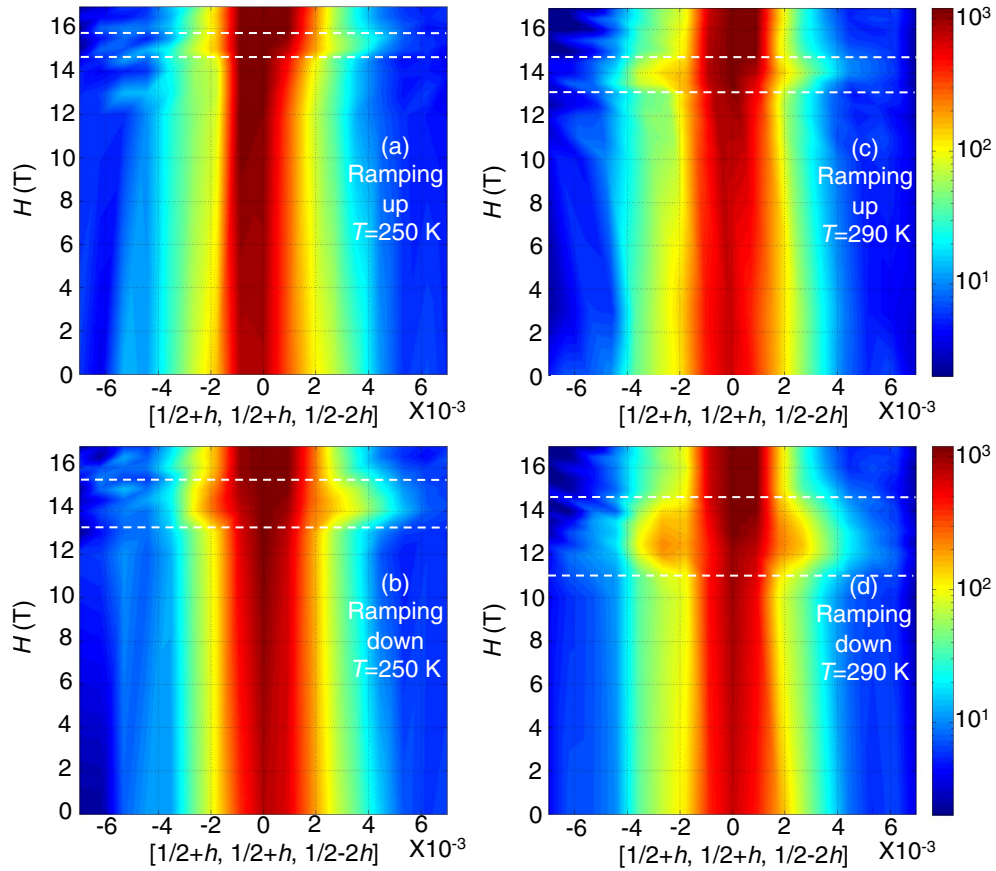


FIG. 4. Contour plots of the magnetic intensities at $(1/2 \pm h, 1/2 \pm h, 1/2 \mp 2h)$ with $H \parallel [1, 1, -2]$ during magnetic field increasing (a) and decreasing (b) processes at 250 K. (c) and (d) The results at 290 K. Two broken lines show the field region where incommensurate peaks are observed.

is either commensurate or splits along the magnetic field direction. The current measurements clarify that there are both commensurate and incommensurate peaks in the IM phase. The commensurate peak originates from the almost collinear antiferromagnetic component perpendicular to the field, although it is slightly canted to the field direction. Since we could only access one set of incommensurate magnetic Bragg peaks around $(1/2, 1/2, 1/2)$, it is difficult to determine the magnetic structure uniquely. There are two possible magnetic structures. One is the AF cone structure, in which the incommensurate peaks originate from the cycloidal component with the easy plane perpendicular to $[1, -1, 0]$, as shown in Fig. 1(b). The other is the fan structure, in which the incommensurate peaks originate from the spin-density-wave component along the field direction, and the spins oscillate around $[1, -1, 0]$ direction in the $[1, -1, 0]$ - $[1, 1, -2]$ plane. Since the DM interactions, which can give rise to the AF cone structure, are present [20], the AF cone structure is considered to be an appropriate structure for the IM phase.

The commensurate and incommensurate magnetic Bragg intensities as well as the magnetization [16] shows a hysteretic behavior between the field increasing and decreasing processes, indicating that the transition from the cycloid to AF cone phase is of first order. Therefore, in the magnetic field range where the incommensurate signal from the AF cone structure is negligible at the lower field side of the phase

boundary, the commensurate intensity probably originates mostly from the cycloid phase and slightly from the collinear component of the AF cone phase. On the other hand, in the magnetic field range where the incommensurate signal from the AF cone structure is finite, the commensurate intensity probably originates mostly from the collinear component of the AF cone phase. In the latter field range we calculated the cone angle of the AF cone structure from the ratio of the commensurate and incommensurate intensities $\tan^{-1}(\sqrt{I_C}/I_C)$, where I_C is the integrate intensity of the two incommensurate magnetic peaks and I_C is the integrate intensity of the commensurate magnetic peak. The cone angle as a function of magnetic field is shown in Figs. 5(c) and 5(d). The cone angles are very similar both in the field increasing and decreasing processes and it decreases gradually at the higher field phase boundary of the AF cone structure. However, it is clearly seen that the AF cone phase is expanded to the lower fields in the field decreasing process and the cone angle becomes much larger around the lower field phase boundary.

The fact that the transition from the cycloid to AF cone phase is of first order suggests that a structural distortion is related to the magnetic field induced transition to the AF cone phase. A hysteretic behavior of the magnetostriction was actually reported in Ref. [16]. The lattice elongation is more enhanced in the field decreasing process. Interestingly, the cycloidal component is more enhanced so that the cone angle

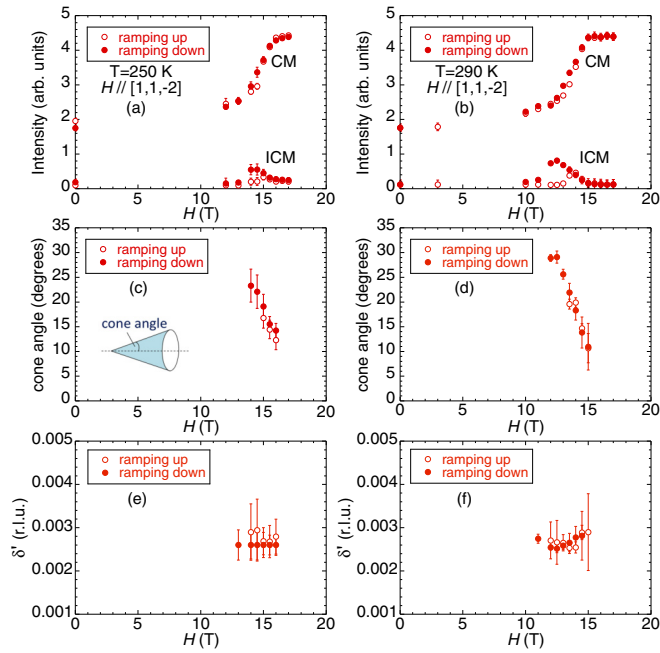


FIG. 5. Integrated intensities of the commensurate (CM) and two incommensurate magnetic (ICM) peaks as a function of magnetic field at 250 K (a) and 290 K (b). Filled and open circles represent the intensities measured during the field increasing and decreasing processes, respectively. (c) and (d) Cone angle as a function of magnetic field at 250 and 290 K, respectively. (e) and (f) Incommensurability (δ') as a function of magnetic field at 250 and 290 K, respectively.

becomes larger in the field decreasing process, as shown in Figs. 5(c) and 5(d). This indicates that the AF cone structure is strongly coupled to the structural distortion. The strong magnetoelectric coupling reported in the AF cone phase [16] can be ascribed to this magnetoelastic coupling. Since the cycloidal component is more enhanced at 290 K than at 250 K, the magnetoelectric coupling can be stronger at higher temperatures.

The incommensurability of the magnetic peaks corresponds to the inverse periodicity of cycloidal modulation. The incommensurate peak positions are $(1/2 \pm \delta, 1/2 \mp \delta, 1/2)$ with $\delta = 0.00447(4)$ at 0 T at 295 K [5] and $(1/2 \pm \delta', 1/2 \pm \delta', 1/2 \mp 2\delta')$ with $\delta' = 0.0028(3)$ at 14 T at 290 K in the field decreasing process. In order to compare the incommensurabilities, these values are converted to the same unit (\AA^{-1}), $\sqrt{2}\delta = 0.00632(6)$ [$= 0.00993(9) \text{\AA}^{-1}$] at 0 T and $\sqrt{6}\delta' = 0.0068(7)$ [$= 0.011(1) \text{\AA}^{-1}$] at 14 T. This indicates that the magnetic modulation period is kept at a similar value at the field-induced transition from the cycloid to AF cone phases. Therefore, at the critical field, only the direction of the magnetic wave vector and the easy plane of the cycloid structure rotates by 90 deg without changing the cycloidal modulation period. As described above, δ' is almost magnetic field independent in the AF cone phase. Furthermore, the incommensurate magnetic intensity at the higher field side of the AF cone phase changes gradually. These results suggest that the cone angle gradually changes to zero toward the critical field between the AF cone and CAFM phases, without changing the cycloidal modulation period.

Figures 5(a) and 5(b) show that the intensity of the commensurate peak increases abruptly around 14 and 13 T and finally becomes saturated above 16 and 15 T at 250 and 290 K, respectively. The saturated intensity is about 2.5 times larger than the intensity at 0 T. The increase of the commensurate peak mostly originates from the fact that neutron scattering probes the components of the magnetic moment perpendicular to the wave-vector transfer. Since the measurements were performed at $(1/2, 1/2, 1/2)$, the magnetic intensity becomes maximum when the magnetic moments point perpendicular to $[1, 1, 1]$. In the CAFM structure [Fig. 1(c)] the magnetic moments point almost perpendicular to $[1, 1, 1]$. On the other hand, only half of the magnetic moments point along $[1, 1, 1]$ in the cycloid phase [Fig. 1(a)]. Therefore, the intensity should become two times larger at the CAFM phase, which is slightly smaller than the enhancement factor actually observed. In order to explain this difference, we should consider a puzzling feature that the commensurate intensity starts to increase slightly around 5 T which is well below the critical field to the IM phase. The increase of the commensurate intensity is also observed in the different configuration, as described in Sec. III A [Fig. 3(b)]. These results indicate that the slightly increasing signal is commensurate and exactly centered at $(1/2, 1/2, 1/2)$. One possibility is that a tiny fraction of the CAFM component appears at low fields. Another possibility is that a structural distortion gives rise to a superlattice peak at $(1/2, 1/2, 1/2)$. The latter explains the larger enhancement factor. However, this is outside of the scope of this paper and a further study is needed to clarify the origin of the additional commensurate peak.

IV. SUMMARY

Neutron diffraction measurements in BiFeO_3 were performed under magnetic field up to 17 T to clarify the magnetic structure in the IM phase. We found that the AF cone structure predicted in Ref. [16] best describes our results. The results give a new insight about the magnetic field induced transitions. The transition from the cycloid to AF cone is of first order and the direction of the magnetic wave vector and the cycloidal plane are rotated by 90 deg without changing the cycloidal modulation period. The transition from the AF cone to CAFM phase is gradual with the cone angle becomes smaller gradually without changing the cycloidal modulation period at the higher field side of the phase boundary. A large hysteretic behavior in the AF cone phase was observed in the cycloidal component in this study and also in the magnetostriction previously reported [16], suggesting a magnetoelastic coupling, which may give rise to a large magnetoelectric effect in the AF cone phase [16]. Furthermore, this effect is found to be more enhanced at higher temperatures, which is ideal for industrial application.

ACKNOWLEDGMENTS

We acknowledge work of the magnet and sample environment groups: S. Gerischer, R. Wahle, S. Kempfer, P. Heller, and P. Smeibidl. This research used resources at the High Flux Isotope Reactor, a DOE Office of Science User Facility operated by the Oak Ridge National Laboratory.

- [1] G. Catalan and J. F. Scott, *Adv. Mater.* **21**, 2463 (2009).
- [2] J.-G. Park, M. D. Le, J. Jeong, and S. Lee, *J. Phys.: Condens. Matter* **26**, 433202 (2014).
- [3] J. R. Teague, R. Gerson, and W. J. James, *Solid State Commun.* **8**, 1073 (1970).
- [4] I. Sosnowska, T. Peterlin-Neumaier, and E. Steichele, *J. Phys. C: Solid State Phys.* **15**, 4835 (1982).
- [5] I. Sosnowska and R. Przenioslo, *Phys. Rev. B* **84**, 144404 (2011).
- [6] M. Ramazanoglu, W. Ratcliff, II, Y. J. Choi, S. Lee, S.-W. Cheong, and V. Kiryukhin, *Phys. Rev. B* **83**, 174434 (2011).
- [7] Y. F. Popov, A. K. Zvezdin, G. P. Vorob'ev, A. M. Kadomtseva, V. A. Murashev, and D. N. Rakov, *Zh. Eksp. Teor. Fiz.* **57**, 65 (1993) [*JETP Lett.* **57**, 69 (1993)].
- [8] A. M. Kadomtseva, Y. F. Popov, G. P. Vorob'ev, and A. K. Zvezdin, *Physica B* **211**, 327 (1995).
- [9] A. M. Kadomtseva, A. K. Zvezdin, Y. F. Popov, A. P. Pyatakov, and G. P. Vorob'ev, *JETP Lett.* **79**, 571 (2004).
- [10] B. Ruetter, S. Zvyagin, A. P. Pyatakov, A. Bush, J. F. Li, V. I. Belotelov, A. K. Zvezdin, and D. Viehland, *Phys. Rev. B* **69**, 064114 (2004).
- [11] J. Park, S.-H. Lee, S. Lee, F. Gozzo, H. Kimura, Y. Noda, Y. J. Choi, V. Kiryukhin, S.-W. Cheong, Y. Jo, E. S. Choi, L. Balicas, G. S. Jeon, and J.-G. Park, *J. Phys. Soc. Jpn.* **80**, 114714 (2011).
- [12] M. Tokunaga, M. Azuma, and Y. Shimakawa, *J. Phys. Soc. Jpn.* **79**, 064713 (2010).
- [13] M. Tokunaga, M. Akaki, A. Miyake, T. Ito, and H. Kuwahara, *J. Magn. Magn. Mater.* **383**, 259 (2015).
- [14] M. Tokunaga, M. Akaki, T. Ito, S. Miyahara, A. Miyake, H. Kuwahara, and N. Furukawa, *Nat. Commun.* **6**, 5878 (2015).
- [15] K. Ohoyama, S. Lee, S. Yoshii, Y. Narumi, T. Morioka, H. Nojiri, G. S. Jeon, S.-W. Cheong, and J.-G. Park, *J. Phys. Soc. Jpn.* **80**, 125001 (2011).
- [16] S. Kawachi, A. Miyake, T. Ito, S. E. Dissanayake, M. Matsuda, W. Ratcliff, II, Z. Xu, Y. Zhao, S. Miyahara, N. Furukawa, and M. Tokunaga, *Phys. Rev. Mater.* **1**, 024408 (2017).
- [17] M. Matsuda, R. S. Fishman, T. Hong, C. H. Lee, T. Ushiyama, Y. Yanagisawa, Y. Tomioka, and T. Ito, *Phys. Rev. Lett.* **109**, 067205 (2012).
- [18] R. S. Fishman, J. T. Haraldsen, N. Furukawa, and S. Miyahara, *Phys. Rev. B* **87**, 134416 (2013).
- [19] J. Jeong, M. D. Le, P. Bourges, S. Petit, S. Furukawa, S.-A. Kim, S. Lee, S.-W. Cheong, and J.-G. Park, *Phys. Rev. Lett.* **113**, 107202 (2014).
- [20] M. Ramazanoglu, M. Laver, W. Ratcliff, II, S. M. Watson, W. C. Chen, A. Jackson, K. Kothapalli, S. Lee, S.-W. Cheong, and V. Kiryukhin, *Phys. Rev. Lett.* **107**, 207206 (2011).
- [21] T. Ito, T. Ushiyama, Y. Yanagisawa, R. Kumai, and Y. Tomioka, *Cryst. Growth Design* **11**, 5139 (2011).
- [22] O. Prokhnenko, P. Smeibidl, W.-D. Stein, M. Bartkowiak, and N. Stüsser, *J. Large-Scale Res. Facilities* **3**, A115 (2017).
- [23] O. Prokhnenko, W.-D. Stein, H.-J. Bleif, M. Fromme, M. Bartkowiak, and T. Wilpert, *Rev. Sci. Instrum.* **86**, 033102 (2015).
- [24] S. Lee, W. Ratcliff, II, S.-W. Cheong, and V. Kiryukhin, *Appl. Phys. Lett.* **92**, 192906 (2008).
- [25] M. Ramazanoglu, W. Ratcliff, II, H. T. Yi, A. A. Sirenko, S.-W. Cheong, and V. Kiryukhin, *Phys. Rev. Lett.* **107**, 067203 (2011).
- [26] S. Bordács, D. G. Farkas, J. S. White, R. Cubitt, L. DeBeer-Schmitt, T. Ito, and I. Kézsmárki, *Phys. Rev. Lett.* **120**, 147203 (2018).